Int. J. Electrochem. Sci., 13 **(2018)** 4504 – 4511, doi: 10.20964/2018.05.64

International Journal of
ELECTROCHEMICAL
SCIENCE
www.electrochemsci.org

Improved Electrochemical Performances of Carbon-coated Li_2MoO_3 Cathode Materials for Li-ion Batteries

Zhiyong Yu[*], *Tianlang Yu, Wenji Li, Jishen Hao, Hanxing Liu, Nian Sun, Mengyun Lu, Juan Ma*

School of Materials Science and Engineering, Wuhan University of Technology,
Wuhan, 430070, P. R. China
[*]E-mail: yuzhiyong@whut.edu.cn

Received: 14 January 2018 / *Accepted:* 8 March 2018 / *Published:* 10 April 2018

Layer-structured oxide Li_2MoO_3 was surface modified via a facile ball-milling followed by heat treatment to obtain carbon-coated materials with enhanced electrochemical performances. The samples were characterized through XRD, SEM, TEM, Raman spectroscopy, charge-discharge and EIS measurements. The structural and morphological characterization confirmed that Li_2MoO_3 particles were successfully covered with nano-sized carbon layer, and the coating of carbon had no obvious effect on the crystal structure of Li_2MoO_3. Charge-discharge tests demonstrated that the carbon-coated materials presented improved reversible capacities, cyclability and rate capability compared to the pristine Li_2MnO_3. EIS results revealed the enhanced electrochemical performances would contribute to the carbon coating layer, which could decrease the charge transfer resistance upon cycling.

Keywords: Li_2MoO_3, Carbon coating, Electrochemical performance, Li-ion battery, Cathode Material

1. INTRODUCTION

With the ever-growing demands of high-density lithium ion batteries, there has been increasing interest to develop cathode materials with high specific capacity. In the ongoing search for higher capacity cathode materials than $LiCoO_2$ or $LiNi_{1/3}Co_{1/3}Mn_{1/3}O_2$, considerable efforts have been focused on lithium-rich layered materials Li_2MnO_3-$LiMO_2$ (M=Mn, Ni, and Co, etc.) with reversible capacities over 250 $mAhg^{-1}$[1-6]. However, the Li_2MnO_3-$LiMO_2$ series suffer from some drawbacks such as large irreversible capacity loss in the initial cycle, fast voltage fading during cycling due to oxygen evolution and structural degradation [2-4]. Therefore, much work has been made to seek the replacement of Li_2MnO_3 with other lithium-rich layered oxides Li_2MO_3 (M=Mo, Ru, Ir, Sn, Ti, etc.) [7-17]. Among them, Li_2MoO_3 has been extensively investigated owing to its high theoretical capacity of 339 $mAhg^{-1}$ [7-12]. However, the low electronic conductivity of Li_2MoO_3 may hinder the charge

transfer and thus result in poor rate performance [10, 11]. Metal ions doping and carbon coating have been confirmed as effective methods to enhance the electrochemical performances of electrode materials with low electronic conductivity [18-22]. Recently, partial substitutions of the transition metal Mo with Cr [9], Fe [12] have been reported to enhance the electrochemical performance of Li_2MoO_3. However, there was little work concerning the impact of carbon coating on the electrochemical performances of Li_2MoO_3. Here, we prepare carbon-coated Li_2MoO_3 cathode materials by using glucose as carbon source via a facile solid-state method. The impacts of carbon coating on the crystal structure, morphology and electrochemical behaviors are studied.

2. EXPERIMENTAL

2.1 Materials synthesis

Layered oxide Li_2MoO_3 was synthesized from Li_2MoO_4 (Alfa Aesar, 99+ %), which was ground and reduced in a stream of dry H_2/N_2 (5:95 v/v) at 700 °C for 48 h. To coat Li_2MoO_3 with carbon, glucose (as the carbon source) and Li_2MoO_3 powder were mixed by ball-milling and then calcined at 700 °C for 2 h under the atmosphere of H_2/N_2 (5:95 v/v). The weight ratio of glucose to Li_2MoO_3 was adjusted to 0%, 5%, 10%, 15% and 20%, and the corresponding samples were referred to as 0G, 5G, 10G, 15G and 20G, respectively.

2.2 Characterization

The phase structure of the pristine and carbon-coated Li_2MoO_3 materials was analyzed by X-ray diffraction (XRD, X'Pert, PANalytical). For observation of morphology and microstructure of the obtained samples, scanning electron microscopy (SEM) and transmission electron microscopy (TEM) were performed on S-4800 and JEM-2100F. Raman measurement was recorded in a Renishaw inVia Raman Microscope using 532 nm laser.

2.3 Electrochemical measurements

The tested coin-cells were assembled with cathode electrode (Li_2MoO_3: carbon black: PVDF=70: 20: 10), anode electrode (lithium foil), one layer of separator (Celgard) and the electrolyte (1 M $LiPF_6$ in EC/DMC= 1/1 in volume). Charge-discharge data of the cells were recorded by battery test system (CT2001A, Land) between 1.5V and 4.5 V. The electrochemical impedance spectroscopy (EIS) analysis was conducted through an electrochemical workstation (CHI660B, Chenhua) ranging from 0.01Hz to 10^5 Hz with the amplitude of 5 mV.

3. RESULTS AND DISCUSSION

XRD patterns of the samples with various amounts of glucose are shown in Fig. 1. The diffraction peaks of as-prepared Li_2MoO_3 could be indexed to the α-$NaFeO_2$ structure with space group R-3m. No obvious impurities or secondary phase are observed in the patterns of glucose modified

samples. The results suggest that the surface treatment has no apparent influence on the phase structure of Li_2MoO_3. The absence of diffraction peaks corresponding to the carbon may be due to the amorphous state or low content of the carbon.

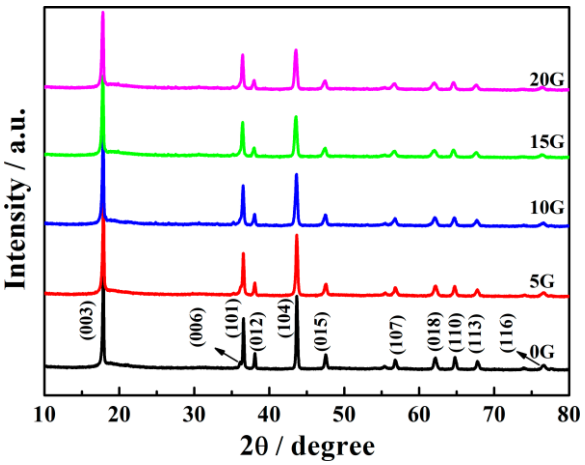

Figure 1. XRD patterns of the samples with various amounts of glucose

Fig. 2 displays the SEM images of all samples. Obviously, there is some difference in morphology for the particles before and after glucose modification. The pristine sample is composed of irregular elongated particles with width in the range of 1~2 μm. After modified by glucose, primary particle sizes of Li_2MoO_3 reduce, which is agreed well with previous results as have been reported in $LiFePO_4$ [23]. The particle aggregation tends to become more serious with an increase in glucose amount, indicating that the more glucose is, the more particles might bond together by carbon formed during heating treatment.

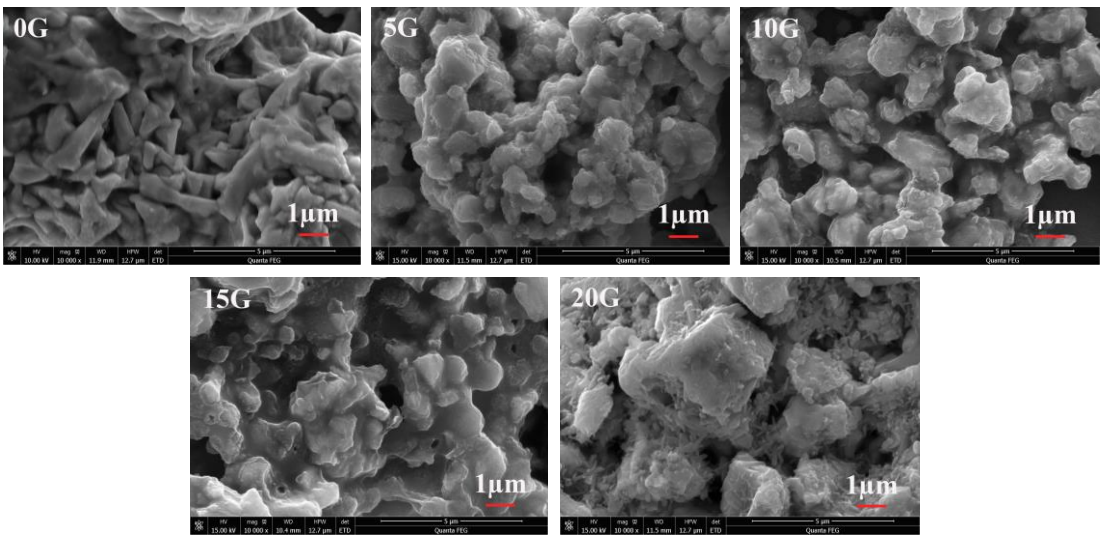

Figure 2. SEM images of the samples with various amounts of glucose

The morphology and state of surface carbon were investigated by TEM and Raman measurements. Fig. 3a-b exhibit the TEM images of 5G and 15G samples. The nano-scale amorphous carbon layers can be detected on the surface of Li_2MoO_3 particles for all samples. Compared to the carbon shell in 5G sample, the shell in 15G sample shows better continuity and uniformity. The thickness of the coated carbon shell derived from glucose is ~10 nm for 15G sample. The Raman spectroscopy is presented in Fig. 3c. Two main bands around 1330 and 1590 cm^{-1} could be allocated as the D band and G band, respectively. The I_D/I_G ratio (I_D/I_G=1.02) as well as the G-band position indicate the carbon is mainly in amorphous state and is of well electronic conductivity [23-25]. The existence of the carbon shell would play a positive role on the enhancement of the electronic conductivity and be benefit for the improvement of the electrochemical performances of Li_2MoO_3.

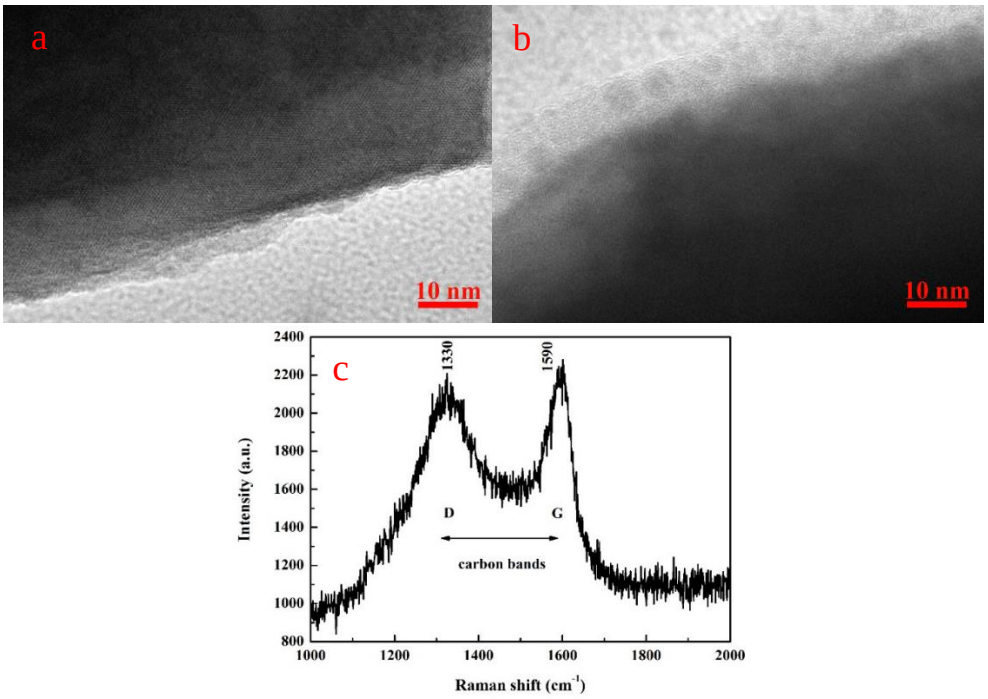

Figure 3. TEM images of 5G (a) and 15G (b) samples, and Raman spectroscopy of 15G (c)

Fig. 4 shows the charge and discharge curves of the initial cycle for all samples between 1.5V and 4.5 V at 5 mAg^{-1}. The carbon coated samples show higher initial discharge capacity than that of the pristine one. Notably, the discharge capacities depend on the amount of glucose. The initial discharge capacities firstly increase and then decrease with an increase of glucose amount. The 15G sample exhibits the highest first discharge capacity of 299.5 $mAhg^{-1}$, while that of pristine sample is only 178.5 $mAhg^{-1}$. Moreover, the difference of the charge and discharge potentials decreases after carbon-coating, which should be mainly due to the increase of the electronic conductivity by coating carbon on Li_2MoO_3. In addition, the initial coulombic efficiency of pure Li_2MoO_3 is only 86%, while the coulombic efficiency of all carbon coated samples exceeds 100% for the first cycle. For coating carbon, the ball-milling process was carried out under air in the present work. As previous report, the

surface of Li_2MoO_3 could be oxidized to Li_2CO_3, Li_2MoO_4 and MoO_3 after air exposure [10]. The formation of MoO_3 will lead to a reduction of charge capacity and an increment of discharge capacity for the first cycle, therefore the coated samples show higher initial coulombic efficiency. The initial charge/discharge capacities of Li_2MoO_3/C in this work and some other Li_2MO_3 based materials in previous literatures are listed in Table 1. As listed, Li_2MoO_3/C composite delivers high charge/discharge capacities, implying carbon coating is a profitable method to enhance the specific capacities of Li_2MoO_3.

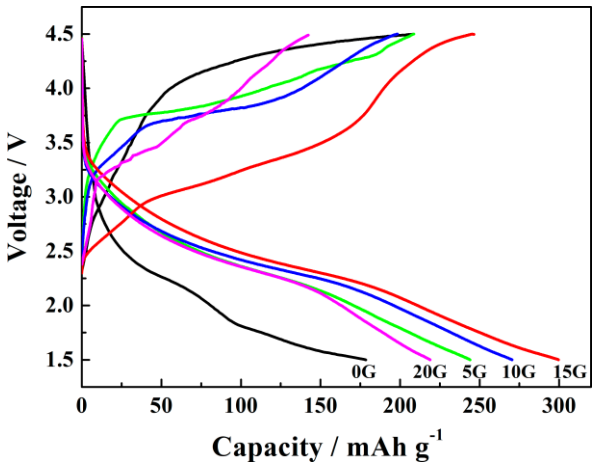

Figure 4. The initial charge and discharge curves of the pristine and carbon-coated Li_2MoO_3 samples at 5 mAg^{-1}

Table 1. The initial charge/discharge capacities of Li_2MoO_3/C in this work and some other Li_2MO_3 based materials in previous literatures

Cathode materials	Charge capacity ($mAhg^{-1}$)	Discharge capacity ($mAhg^{-1}$)	Voltage (V)	Ref.
$Li_{1.211}Mo_{0.467}Cr_{0.3}O_2$/C	-	265.4	1.5-4.3	9
Li_2MoO_3	-	210	2.0-4.5	11
$0.9Li_2MoO_3$-$0.1LiFeO_2$	235	139.5	1.5-4.4	12
$Li_2Ru_{0.75}Ti_{0.25}O_3$	-	240	2.0-4.6	14
Li_2RuO_3	-	250	2.0-4.6	15
$Li_2Ru_{0.75}Sn_{0.25}O_3$	-	230	2.0-4.6	15
Li_2IrO_3	-	190	2.0-4.8	17
Li_2MoO_3/C (15G)	246.5	299.5	1.5-4.5	This work

Fig. 5 presents the cycling performance of all samples at 20mAg^{-1} between 1.5V and 4.5 V. As shown in Fig. 5, the initial capacity of 15G sample is 239.4 $mAhg^{-1}$ at 20 mAg^{-1}, which increases by 131.1% compared with the capacity of sample without carbon coating. Moreover, the capacity decay rate of the carbon-coated Li_2MoO_3 is less than the pristine one. For example, the discharge capacity of 0G sample is 103.6 $mAhg^{-1}$ in the first cycle and fades to 46.8 $mAhg^{-1}$ in the 50th cycle, corresponding to a capacity decay of 54.8%; The discharge capacities of the 5G, 10G, 15G and 20G are 163.0, 181.6, 238.7 and 126.2 $mAhg^{-1}$ in the first cycle and decrease to 75.5, 119.2, 184.3 and 60.1 $mAhg^{-1}$ after

50th cycle, corresponding to the capacity decay of 53.7%, 34.4%, 22.8% and 52.4%, respectively. The improved cycling performance might contribute to the amorphous carbon coating, which could act as protection layer to suppress the electrode/electrolyte side reactions during cycling.

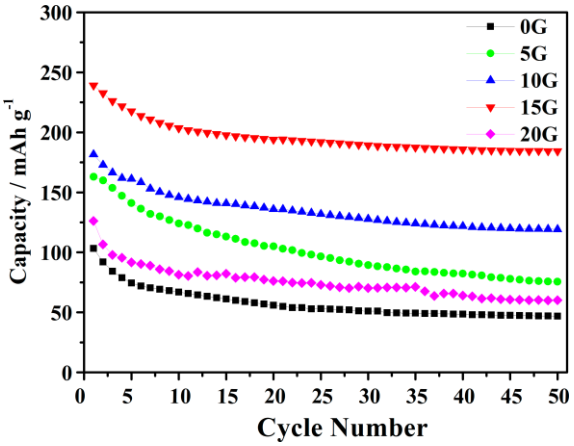

Figure 5. Cycling performance of the pristine and carbon-coated Li_2MoO_3 samples at 20 mAg^{-1}

The rate performance of the 0G and 15G samples is presented in Fig. 6. The cells were cycled from 5mAg^{-1} to 20 mAg^{-1} and each rate kept for fifteen cycles between 1.5V and 4.5V. As observed, the 15G sample displays improved rate performance in the range of tested C-rate. At all C-rate, 15G sample exhibits higher discharge capacities and the capacity-gaps between 0G and 15 G samples become wider with increasing current density. That could be attributed to the carbon shell, which improves the electrical conductivity of layered Li_2MnO_3 material.

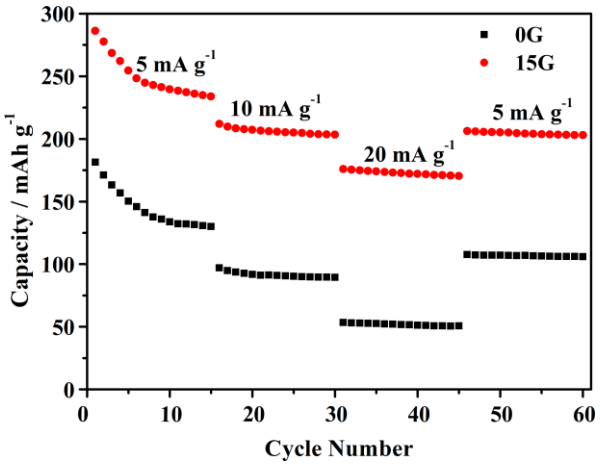

Figure 6. Rate capability of the 0G and 15G samples

EIS measurements were performed for the pristine and 15G samples at fully discharge state after the electrodes were activated 20 cycles (see Fig. 7). The obtained data are fitted using the equivalent circuit (see insert of Fig. 7), which includes the ohmic resistance (R_s), the surface film resistance (R_{SEI}), the charge transfer resistance (R_{ct}). As listed in Table 2, the R_s values show little

difference. However, the 15G sample shows smaller R_{ct} value comparing to the pristine one, explaining the higher capacity and better rate performance of 15G sample in Fig. 4-6. Table 2 also shows that all the R_{SEI} values are small. Even so, R_{SEI} value still decreases by coating the Li_2MoO_3 with carbon, suggesting that the resistance of Li-ion migration decreases. All above results suggest that appropriate carbon coating cause an enhancement of conductivity and would be favorable for the improvement of electrochemical performances of Li_2MoO_3.

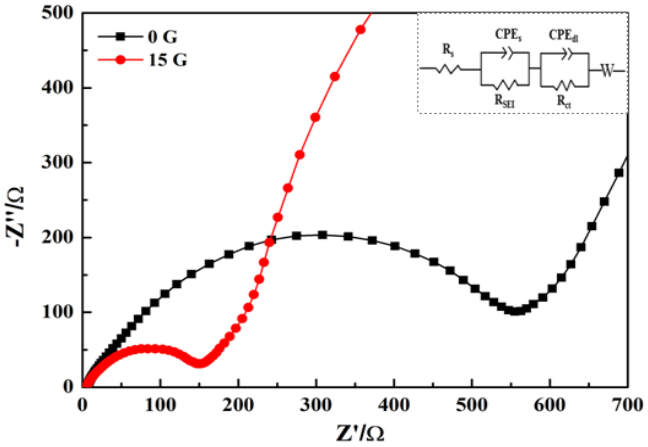

Figure 7. Nyquist plots of pristine and 15G samples. Inset: Equivalent circuit

Table 2. Impedance parameters calculated based on equivalent circuit

Samples	R_s (Ω)	R_{SEI} (Ω)	R_{ct} (Ω)
0G	6.028	13.31	597
15G	5.687	1.041	160.9

4. CONCLUSIONS

In summary, carbon-coated Li_2MoO_3 cathode materials were prepared by a facile ball-milling followed by heat treatment. The impacts of carbon coating on the structure and electrochemical behaviors of Li_2MoO_3 were studied. XRD demonstrated that the carbon coating did not influence the phase structures of the materials. TEM and Raman tests showed that the samples with glucose were coated with a nano-sized carbon layer. The surface coating of carbon leaded to the significant enhancement in the specific capacity, cycling stability and rate capability of Li_2MoO_3. Such an improvement could owe the lower charge transfer resistance to the enhancement of the electronic conductivity and the diminishment of the cathode/electrolyte side reactions resulting from the carbon shell on the surface of Li_2MoO_3.

ACKNOWLEDGEMENTS
This work was supported by Natural Science Foundation of China (No. 51372191 and No. 51102189) and the Fundamental Research Funds for the Central Universities (WUT: 2015III063).

References

1. M.A. Mezaal, L. Qu, G. Li, W. Liu, X. Zhao, K. Zhang, R. Zhang, L. Lei, *J. Solid State Electrochem.*, 21 (2017) 145.
2. C.J. Chen, W.K. Pang, T. Mori, V.K. Peterson, N. Sharma, P.H. Lee, S.H. Wu, C.C. Wang, Y.F. Song, R.S. Liu, *J. Am. Soc.*, 138 (2016) 8824.
3. J. Li, J. Camardese, R. Shunmugasundaram, S. Glazier, Z. Lu, J.R. Dahn, *Chem. Mater.*, 27 (2015) 3366.
4. C.R. Fell, D. Qian, K.J. Carroll, M. Chi, J.L. Jones, Y.S. Meng, *Chem. Mater.*, 25 (2013) 1621.
5. E.S. Lee, A. Huq, H.Y. Chang, A. Manthiram, *Chem. Mater.*, 24 (2012) 600.
6. M.M. Thackeray, S.H. Kang, C.S. Johnson, J.T. Vaughey, R. Benedek, S.A. Hackney, J. *Mater. Chem.*, 17 (2007) 3112.
7. M. Tian, Y. Gao, R. Xiao, Z. Wang, L. Chen, *Phys. Chem. Chem. Phys.*, 19 (2017) 17538.
8. X. Hu, W. Zhang, X. Liu, Y. Mei, Y. Huang, *Chem. Soc. Rev.*, 44 (2015) 2376.
9. J. Lee, A. Urban, X. Li, D. Su, G. Hautier, G. Ceder, *Science*, 343 (2014) 519.
10. J. Ma, Y. Gao, Z. Wang, L. Chen, *J. Power Sources*, 258 (2014) 314.
11. J. Ma, Y.N. Zhou, Y. Gao, X. Yu, Q. Kong, L. Gu, Z. Wang, X.Q. Yang, L. Chen, *Chem. Mater.*, 26 (2014) 3256.
12. K.S. Park, D. Im, A. Benayad, A. Dylla, K.J. Stevenson, J.B. Goodenough, *Chem. Mater.*, 24 (2012) 2673.
13. S. Liu, J. Wang, Z. Tian, Q. Li, X. Tian, Y. Cui, Y. Yang, *Chem. Commun.*, 53 (2017) 11913.
14. M. Sathiya, G. Rousse, K. Ramesha, C.P. Laisa, H. Vezin, M.T. Sougrati, M.L. Doublet, D. Foix, D. Gonbeau, W. Walker, A.S. Prakash, M. Ben Hassine, L. Dupont, J. M. Tarascon, *Nat. Mater.*, 12 (2013) 827.
15. M. Sathiya, A.M. Abakumov, D. Foix, G. Rousse, K. Ramesha, M. Saubanère, M.L. Doublet, H. Vezin, C.P. Laisa, A.S. Prakash, D. Gonbeau, G. VanTendeloo, J.M. Tarascon, *Nat. Mater.*, 14 (2015) 230.
16. B. Li, R. Shao, H. Yan, L. An, B. Zhang, H. Wei, J. Ma, D. Xia, X. Han, *Adv. Funct. Mater.*, 26 (2016) 1330.
17. P.E. Pearce, A.J. Perez, G. Rousse, M. Saubanère, D. Batuk, D. Foix, E. McCalla1, A.M. Abakumov, G.V. Tendeloo, M.L. Doublet, J.M. Tarascon, *Nat. Mater.*, 16 (2017) 580.
18. Q. Cheng, W. He, X. Zhang, M. Li, L. Wang, *J. Mater. Chem. A*, 5 (2017) 10772.
19. J. Wang, X. Sun, *Energy Environ. Sci.*, 5 (2012) 5163.
20. H. Li, H. Zhou, *Chem. Commun.*, 48 (2012) 1201.
21. T. Muraliganth, K.R. Stroukoff, A. Manthiram, *Chem. Mater.*, 22, (2010) 5755.
22. M.M. Doeff, J.D. Wilcox, R. Kostecki, G. Lau, *J. Power Sources*, 163 (2006) 180.
23. C. Miao, P. Bai, Q. Jiang, S. Sun, X. Wang, *J. Power Sources*, 246 (2014) 232.
24. A.C. Ferrari, J. Robertson, *Phil. Trans. R. Soc. Lond. A*, 362 (2004) 2477.
25. X. Wang, Z. Feng, J. Huang, W. Deng, X. Li, H. Zhang, Z. Wen, *Carbon*, 127 (2018) 149.